SAND2009-0138C

Turbulence Structure in Oscillating Channel Flow

Sean P. Kearney[1], Timothy J. O'Hern[2], Thomas W. Grasser[3], and Thomas G. Dimiduk[4]
Sandia National Laboratories, Albuquerque, New Mexico, 87185

Jesse D. Roberts[5]
Sandia National Laboratories, Carlsbad, New Mexico, 88220

and

Joseph Z. Gailani [6]
United States Army Corps of Engineers, Vicksburg, MS, 39180

The structure of turbulence in an oscillating channel flow with near-sinusoidal fluctuations in bulk velocity is investigated. Phase-locked particle-image velocimetry data in the streamwise/wall-normal plane are interrogated to reveal the phase-modulation of two-point velocity correlation functions and of linear stochastic estimates of the velocity fluctuation field given the presence of a vortex in the logarithmic region of the boundary layer. The results reveal the periodic modulation of turbulence structure between large-scale residual disturbances, relaminarization during periods of strong acceleration, and a quasi-steady flow with evidence of hairpin vortices, which is established in the acceleration phase and persists through much of the deceleration period.

I. Introduction

PERIODICALLY unsteady wall-bounded flows are important in a wide range of engineering and medical applications, including sediment transport and ocean engineering [1], flow in the human circulatory system, and enhanced heat transfer [2]. For the canonical problem of fully developed channel/pipe flow, analytical solutions exist for sinusoidal time variations in pressure gradient [3, 4] or volume flow rate [5, 6], and the problem is well-understood. In the turbulent regime, experimental data that describe the time-dependent evolution of the phase-locked, Reynolds-averaged velocity field statistics have been provided [7-10], and these experimental data are complimented by more recent reports of LES/DNS simulations [11-13]. Reynolds-averaged information is a useful descriptor of turbulent fields, but does not always yield the needed insight into the fundamental dynamics of the flow that is given by the identification and description of spatially and temporally coherent structures, which have been extensively described in steady turbulent wall flows [14, 15] and have been found to contribute significantly to the production and maintenance of wall turbulence.

The description of the time evolution of coherent structures in periodically unsteady turbulent wall flows (hereafter referred to as "oscillating flows") is less developed than for the steady case, but a picture is beginning to emerge based largely on the results of recent numerical simulations [11-13] and earlier flow visualization experiments [16, 17], which must be verified using a more quantitative experimental description based on direct, and spatially correlated measurement of the velocity field. Earlier measurements in oscillating turbulent wall flows [7-9] utilized point LDV data, from which structural and spatially correlated information cannot be extracted. Our group has recently reported [10] what we believe to be the first PIV measurements in a canonical oscillating wall flow. Our

[1] Principal Member of the Technical Staff, Engineering Sciences Center, PO Box 5800/Mail Stop 0826, Senior Member AIAA, email: spkearn@sandia.gov
[2] Principal Member of the Technical Staff, Engineering Sciences Center
[3] Distinguished Technologist, Engineering Sciences Center
[4] Student intern, present address: Department of Physics, Massachusetts Institute of Technology, Cambridge, MA, 02139
[5] Principal Member of the Technical Staff, Carlsbad Programs Group
[6] Senior Engineer, Engineer Research and Development Center, Coastal and Hydraulics Laboratory

earlier report provided a Reynolds-averaged description of the turbulent field along with a brief, qualitative presentation of the instantaneous 2-D structure of the flow. A portion of our PIV data set is analyzed here to extract quantitative 2-D structural and spatial correlation information, which can then be compared to the present view of turbulence structure in both oscillating and steady turbulent wall flows.

II. Experiment

Particle-Image Velocimetry (PIV) measurements in the streamwise/wall-normal plane were acquired in the SEAWOLF (Sediment Erosion Actuated by Wave Oscillations and Linear Flow) water channel facility, shown in Fig. 1. Oscillating flow in SEAWOLF was provided by a set of reciprocating pistons, which were in communication with opposite ends of the test channel. The channel could be operated in a purely oscillatory mode, with zero time-mean bulk velocity, by closing a metering valve to isolate the test section from the head tanks, which otherwise would provide a well-controlled time-averaged head difference and DC bulk velocity component through the channel. The test channel was 2-m long, and 20-mm high × 105.4-mm wide (aspect ratio = 5.5:1). The 2-m test-section length was limited by space constraints and is short enough that end effects are, admittedly, present, as fluid that begins the forcing cycle at the measurement station leaves and re-enters the test section during the course of a forcing cycle. All PIV measurements were made in a streamwise/wall-normal plane, which was located at the spanwise centerline at a streamwise location of 1 m, or 52.5 channel heights, from the channel ends. For steady flow in the facility, the PIV-measured mean velocity profile was in agreement with the logarithmic law, and the measured wall friction coefficient, C_f, was within 10% of accepted empirical values computed using the well-known Blasius formula, $C_f = 0.0791 Re^{1/4}$, when the Reynolds number was based on the channel hydraulic diameter [18]. Measured phase-locked mean velocity profiles in oscillating flow further exhibited logarithmic behavior during turbulent portions of the cycle and the mean and second-moment velocity statistics [10] displayed similar behavior to reported LDV measurements in oscillating Stokes boundary layers [8, 9].

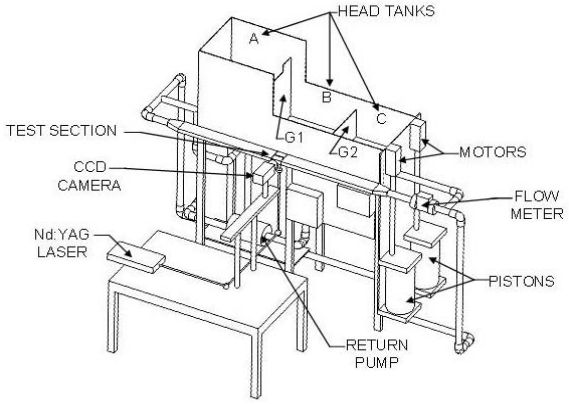

Figure 1. Schematic of the SEAWOLF test facility and PIV Instrumentation

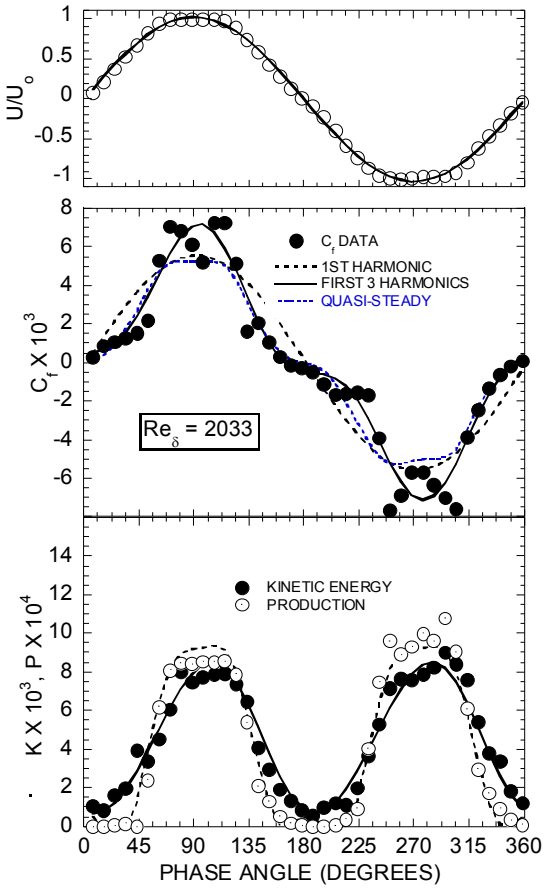

Figure 2. Phase-averaged modulation of bulk velocity (top); wall skin friction (middle); in-plane turbulent kinetic energy and turbulence production integrated across the channel height

A more detailed description of our PIV system has been provided previously [10] and only a summary is provided here. The PIV data were phase locked with respect to the piston motion. Data at forty evenly spaced phase angles were acquired, with 240 velocity realizations acquired at each phase angle (9600 total velocity field realizations for the flow condition reported here). The PIV system used here had the unique feature of a dynamically varying laser pulse delay to accommodate the large, time-dependent swings in the channel bulk velocity. The delay between the illuminating laser pulses was adjusted to keep a nominally 10-15 pixel displacement

between the particle image pairs, based on the metered bulk velocity waveform. Pulse delays were computed for each flow condition and preprogrammed into a custom LabView timing generator, which provided forty independent pulse delays per cycle, as synchronized to a zero trigger from an electro-optical switch that was actuated by the motion of one of the forcing pistons. For the test condition to be discussed here, the period of the piston forcing was 5 seconds, with a $U_o = \pm 100$ cm/s amplitude velocity wave and zero time-mean flow through the channel. These conditions yield a Stokes thickness of $\delta = (2\nu/\omega)^{1/2}$ of 1.23 mm, where, ν is the kinematic viscosity, and ω is the circular forcing frequency. The Reynolds number, Re_δ, was 2033, which is in the "fully turbulent" regime identified by Jensen *et al.* [9]. Bulk-velocity, wall-shear-stress and turbulence production/kinetic energy waveforms for the test case are provided in Fig. 2. Under these conditions, the shear stress varied over a ±7.5-Pa range, such that the minimum size of the viscous length scale was 11 μm, occurring during periods of peak wall shear stress. The spatial resolution of the PIV measurements in the streamwise/wall-normal plane was 160 μm, or 14.5 minimum viscous wall units. This represents a worst-case spatial resolution, as the PIV vector spacing in wall units correspondingly improves for off-peak shear-stress conditions, where the phase-resolved value of the viscous length scale is larger.

III. Results and Discussion

A. Instantaneous Flowfield Structure

Representative instantaneous velocity vector realizations for the first half cycle are shown in Fig. 3. The vector fields are plotted for the lower half of the channel over a streamwise distance, x/H of 1.8, where H is the channel half height. A streamwise convective velocity, U_c, of 85% of the phase-locked mean at the channel centerline has been subtracted from the vector fields to reveal the structure of turbulence in a reference frame which is nominally moving with the near-wall flow. Any organized vortical structure which is traveling at U_c will appear as the closed, circular vector patterns which are associated with vortex motion. The vectors are also plotted on top of gray-scale contours of swirling strength, λ_{ci}, which is an accepted frame-independent kinematic identifier of vortex motion [19] that marks the location of vortices traveling at speeds other than U_c.

At 8˚ and 17˚ the bulk velocity is near zero; reversals of the bulk flow direction and sign of the channel pressure gradient have just occurred. At this time, production of turbulence has ceased (see Fig. 1) and turbulence from the decelerating portion of the previous half cycle that is dominated by large-scale vertical up- and downwash motions persists. Pockets of swirling strength are observed throughout the channel. By 35˚ and 53˚ the impact of strong acceleration is felt throughout the flow. Production remains essentially zero at 35˚ and weak swirling strength events are generally limited to a near-wall region for $y/H < 0.2$; the bulk flow in the core of the channel has essentially relaminarized and the velocity profiles display a flat, "plug flow" behavior. At 53˚ production has begun, with some vertical ejection of swirling motion from the wall observed in some fraction of the realizations, such as the one shown in Fig. 3. The acceleration phase ends near the peak of the velocity wave, where the structure is typical of that seen at 71˚; production is near cycle-peak values, an organized procession of strong vortex cores reminiscent of hairpin vortex signatures [20] appears (more evidence below), and a logarithmic phase-mean velocity profile [10] is established.

During the deceleration portion of the half cycle at 89˚ and 107˚, the flow is in the same quasi-equilibrium state as at 71˚ above, with a succession of vortex cores travelling near U_c, and at an inclined angle to the flow direction, as marked by the white arrows clarifying a succession of swirling strength events for the vector field at 107º. By 125˚, a weak deceleration has initiated. By 161˚, production of turbulence is still nonzero, and organized vortical structures are still observed. The half cycle ends near 179˚, where the mean velocity profile reveals that the flow in the near-wall region has already changed direction, turbulence production has reverted to zero levels and very large-scale, residual turbulence, similar to that observed near the start of the half cycle at 8˚ reappear.

B. Two-Point Spatial Correlations

Statistical imprints of the instantaneous structure discussed above can be realized by computing two-point correlation functions of the velocity fluctuations [21]. The phase evolution of two-point self-

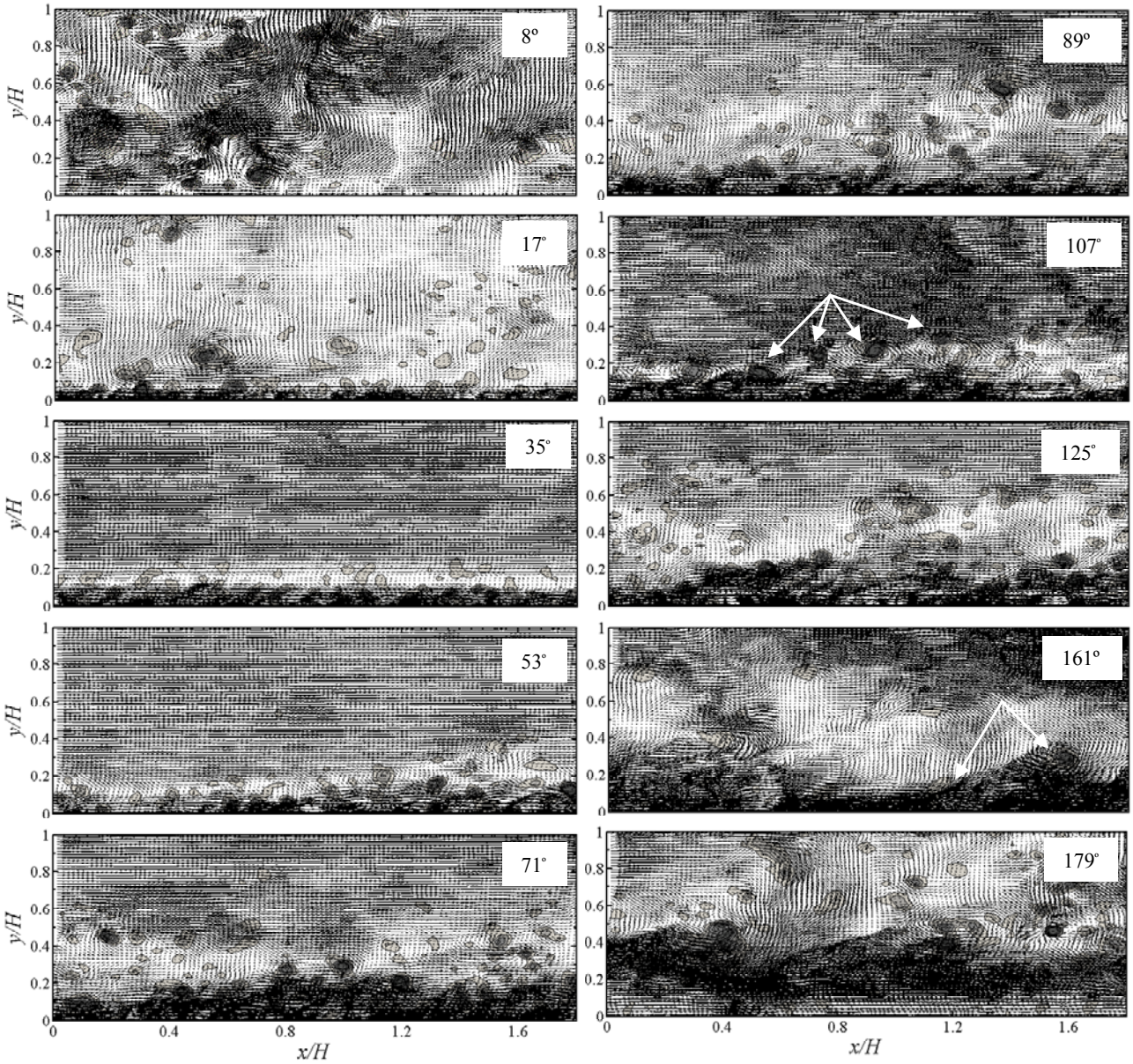

Figure 3. Instantaneous PIV realizations for the accelerating (left) and decelerating (right) portions of the first half cycle.

correlation functions of the streamwise (R_{uu}) and wall-normal (R_{vv}) velocity fluctuation fields were computed from phase-locked velocity fluctuation data using,

$$R_{ij}(r, y; y_o, \theta) = \frac{\left\langle u_i(x, y_o)\, u_j(x+r, y) \right\rangle}{\sigma_i(y_o)\sigma_j(y)} \quad , \tag{1}$$

where the *i,j* subscripts refer to the direction of the velocity components, the u_k represent the velocity component fluctuations about their respective phase-locked means, the σ_k are the rms fluctuations of the u_k, and the $\langle\ \rangle$ brackets represent averaging over the *x* coordinate and the ensemble of 240 phase-locked PIV realizations at phase angle, θ.

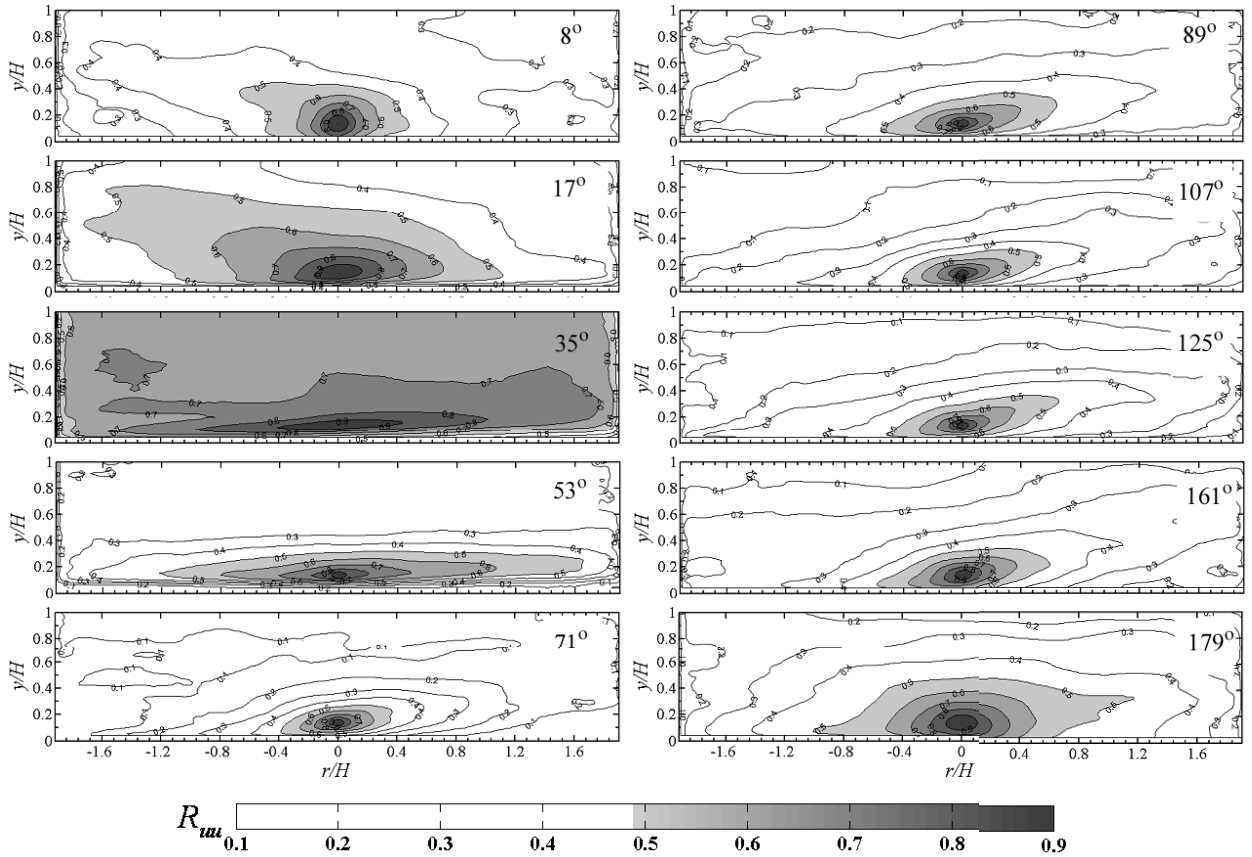

Figure 4. Two-point spatial correlation of the streamwise velocity fluctuations at ten different phase angles over the first half cycle. The event location, y_{ref}, is located at $y/H = 0.137$.

The correlations were computed using a reference height, $y_o = 0.137H$, or a viscous length of $50 < y^+ < 125$, which places the reference point in the log layer (when the flow is turbulent) for the majority of the forcing cycle.

The time evolution of the two-point correlation fields is observed in Figs. 4 and 5, where contour plots of R_{uu} and R_{vv} are shown. The reader should note the different scales on the horizontal axes in Figs. 4 and 5, which were used because the streamwise extent of the R_{uu} correlation was much larger than for R_{vv}. For quick visualization of the mean size and orientation of organized turbulent structure, contours for R values higher than 0.5 are filled with grayscale colors, with lower-valued contours unfilled. The small ensemble size (240 PIV realizations) used to compute the correlations provided only marginal convergence, but this is still sufficient to visualize the streamwise evolution of these quantities. Larger PIV image ensembles, while desirable, were not practical, as the unsteady, phase-locked nature of the experiments was costly, with each run taking 6-8 hours each for setup and acquisition of 200-250 forcing cycles.

Early in the acceleration phase between 8˚ and 35˚, the turbulent fluctuations were correlated over very large spatial extents, and with the R_{uu} contours exhibiting an inclination toward the upstream direction, which persists from the previous half cycle where the bulk-flow direction was reversed. The large spatial extent of both the streamwise and wall-normal velocity correlation fields is associated with the very large up- and downwash structures at 8º and a relaminarized core flow at 17º and 35º, as observed in the instantaneous velocity fields of Fig. 3. The flow is relaminarized at 35˚, where the extent of highly correlated R_{uu} fills the channel half height with diminished size observed in R_{vv}, which we interpret to be a result of cycle-to-cycle jitter in the observed laminar plug flow with essentially zero vertical fluctuation. By 53˚ turbulence production has restarted and a highly elongated R_{uu} is observed, with no significant inclination from the wall. This behavior is consistent with a developing turbulent boundary layer in the near-wall region with a laminar plug flow in the channel core. The elongated R_{uu} correlation is also consistent with recent computational observations of the transition process in oscillating flows [13], where very long streamwise-oriented streaky structures appear in the near-wall region at the initial onset of turbulence production. From 71˚ to 125˚ the R_{uu} and R_{vv} correlations are quantitatively similar to those reported by Christensen *et al.* [21]for steady channel flows at $Re_\tau = 1150$. In the 71˚ to 125˚ time frame, the flow in our channel is near the

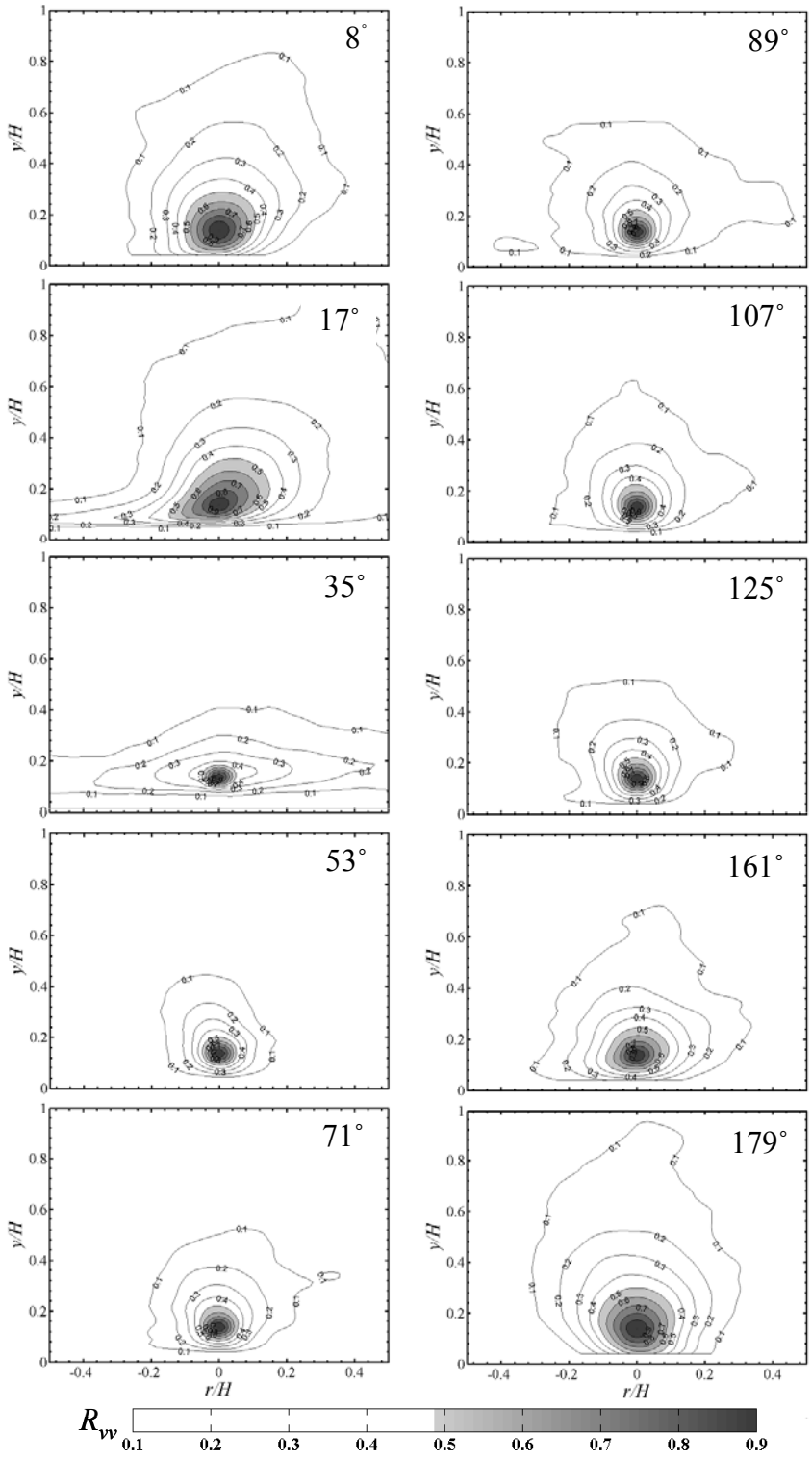

Figure 5. Two-point spatial correlation of the wall-normal velocity fluctuations at ten different phase angles over the first half cycle. The event location, y_{ref}, is located at $y/H = 0.137$.

peak of the bulk velocity waveform shown in Fig. 2, with minimal acceleration and a near-constant wall shear stress, resulting in a quasi-equilibrium value of $Re_\tau = 900$. The $R_{uu} = 0.5$ threshold is ~0.9 H in extent with an upward incline in R_{uu} of ~ 7-13 degrees in our data, compared to 12.5° estimated from Christensens's results [21]. The half cycle then ends with a growth of the extent of both R_{uu} and R_{vv} and the next half cycle then begins with this persistent large-scale turbulence.

C. Conditional Velocity Fields

The two-point spatial correlation fields discussed above provide a picture of the mean size and spatial extent of the turbulent fluctuations, but do not provide any insight regarding the dynamic mechanisms that underlie the development of any organized velocity fluctuations. In steady turbulent wall flows, there has been significant recent evidence to link boundary layer structure and the production/maintenance of Reynolds shear stress to the existence of organized groupings, or "packets," of hairpin vortices [15]. Inspection of many of the instantaneous PIV vector fields of the type shown in Fig. 3 reveals features which are similar to the hairpin-vortex signatures identified in 2-D PIV measurements in steady flows [20]. Specifically, the presence of organized packets of swirling strength, which are inclined at a shallow angle to the flow direction are observed. These regions of swirling strength, as marked by white arrows on two of the realizations in Fig. 3, often demarcate a low-momentum near-wall region from the high-momentum bulk flow. If hairpin vortices are then commonplace in oscillatory wall turbulence, several questions then arise. Are hairpins present? When are they present? How do hairpins grow, develop and dissipate in the presence of strong cyclic acceleration, deceleration, and relaminarization? To begin to address some of these questions we have extended the analysis of Christensen and Adrian [22], in which we compute the expected value of the velocity fluctuation field, given the presence of a near-wall swirling strength event—which may or may not arise from hairpin-vortex motion. This conditionally averaged velocity field is approximated using linear stochastic estimation. The proper form of the linear estimate, as given by Christensen and Adrian [22] is,

$$\left\langle u_j(x+r,y) \middle| \lambda_{ci}(x,y_o) \right\rangle \approx \frac{\left\langle \lambda_{ci}(x,y_o) u_j(x+r,y) \right\rangle}{\left\langle \lambda_{ci}(x,y_o) \lambda_{ci}(x,y_o) \right\rangle} \lambda_{ci}(x,y_o) \quad . \tag{2}$$

From Eq. 2, we can see that the expected velocity field, given the condition of a λ_{ci} event at height y_o from the wall can be computed using the *unconditional* two-point correlation between λ_{ci} and the velocity fluctuation components. The use of unconditional correlation data greatly simplifies the calculation of these estimates by eliminating the need to sample all instantaneous fields for swirling strength events.

Linear estimates of the evolution of the conditional velocity fluctuation fields for a λ_{ci} event at $y_o = 0.137\,H$ for select phase angles over the first half cycle are shown in Fig. 6. The phase angles selected for presentation in Fig. 6 bracket the portion of the half cycle where in-plane signatures of groups of hairpin vortices appear. These 2-D signatures have been described previously by Adrian, Meinhart, and Tomkins [20], and by Christensen and Adrian [22]. Briefly, a hairpin signature in a two-dimensional vector realization occurs with a near-wall swirling strength event, as evidenced by circular vector patterns traveling in the frame of reference of the vortex. This vortex core is further associated with a stagnation line that demarcates upstream Q2 events to the wall-side of the vortex core, and Q4 events to the free-stream side of the vortex. Furthermore, there is recent experimental evidence, as summarized by Adrian [15], which suggests that these vortices travel in organized groups, or "packets," at a shallow inclined angle to the bulk flow direction. The conditional velocity fields in Fig. 6 have been plotted with the vectors normalized to unit magnitude everywhere, so that the existence of closed streamlines and an inclined stagnation line is more readily observable. In all cases, the event vortex core is marked by a dark circle and located at $x/H = 0$ and $y/H = 0.137$. Additional occurrences of close streamlines are further marked by black arrows, and the approximate inclination angle of the visible stagnation line is indicated by a dashed line.

For phase angles ranging from 62 to 143 degrees, the conditional vector fields exhibit a signature that may be expected from packets of hairpin vortices traveling near the wall and largely in the logarithmic layer of this unsteady turbulent flow. The characteristic inclined pattern first begins to appear at 62º, in the later stages of the cycle acceleration phase, when production and turbulent kinetic energy are still rising in the presence of a favorable pressure gradient. At 62º, the conditional field contains more noise, presumably, as a result of fewer organized vortex events; no clear-cut closed streamlines are visible with the exception of the main event vortex, but an inclined feature, representative of a stagnation line is clearly beginning to form. For phase angles ranging from 71º to 143º several vortices displaced to both the upstream and downstream sides of the event vortex are clearly visible, strongly suggesting that an underlying pattern of traveling groups of vortices is a main feature of this complex, turbulent wall flow from the late acceleration stages and well into the cycle deceleration. This type of vortex organization is not

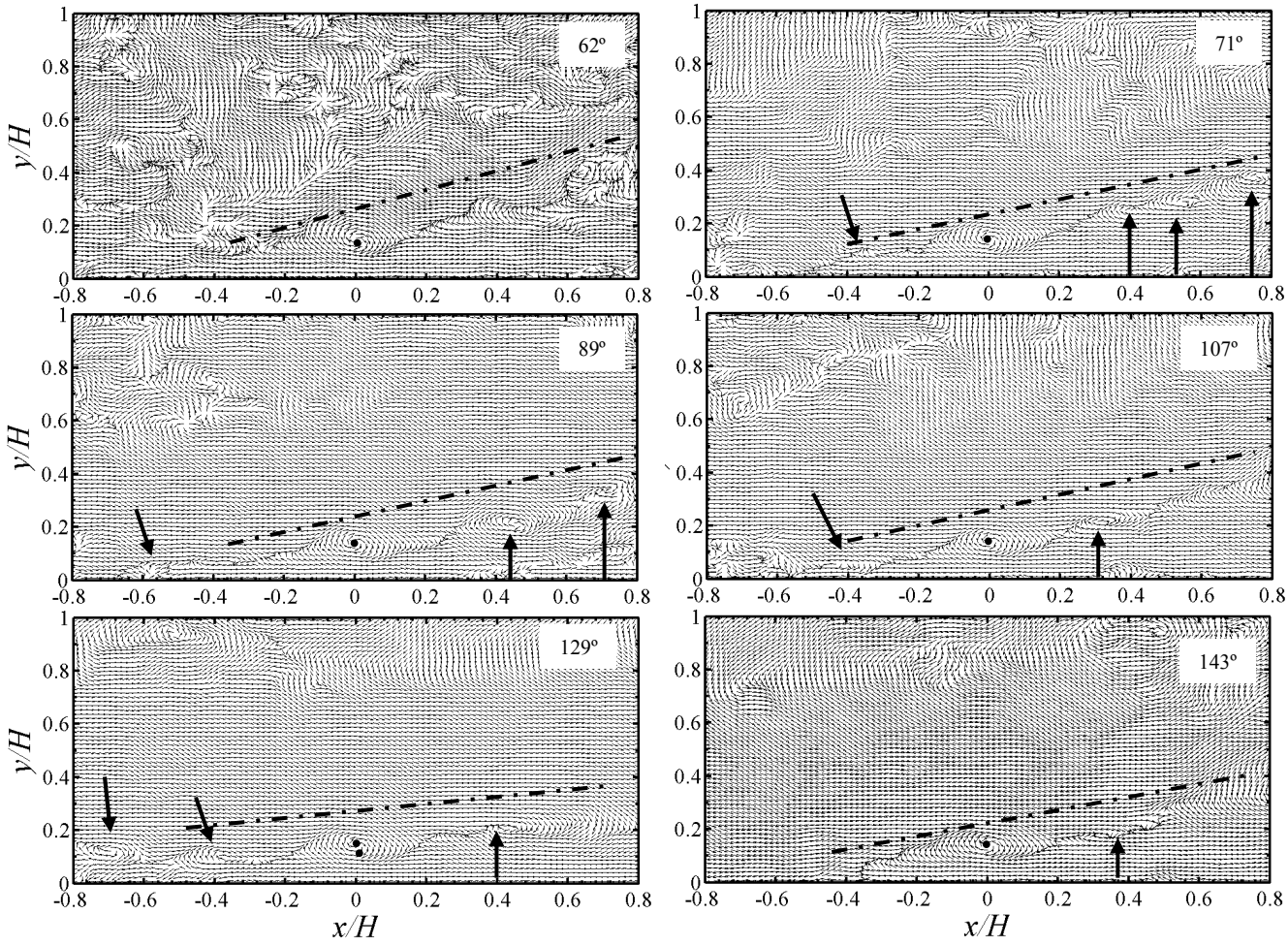

Figure 6. Linear stochastic estimates of the expected velocity field at select phase angles given a λ_{ci} event at $y_{ref}/H = 0.137$ and $x/H = 0$.

apparent during the early acceleration stages, where the flow experiences a very favorable pressure gradient and is in a laminar or transitional state, or in the very late stages of the deceleration phase, where the flow is undergoing a reversal near the wall and the turbulence is substantially weakened. In all cases, an event downstream of the main vortex and displaced by $x/H = 0.4$ is visible, and an additional event displaced by 0.4 in the upstream direction is also observed at phase angles of 62, 71, 107, and 129 degrees. This $x/H \sim 0.4$ vortex spacing was similarly observed in the conditional velocity fields of Christensen and Adrian [21] computed from their PIV results in steady channel flow at $Re_\tau = 547$ and 1734 suggesting insensitivity of the mean vortex spacing to Reynolds number, when scaled with outer units.

IV. Summary and Conclusions

We have presented a detailed analysis of the structure of turbulence in an oscillating channel flow at $Re_\delta = 2033$ using PIV data in the streamwise/wall-normal plane. To our knowledge, this is the first structural information for an oscillating flow derived from direct velocity measurements. The phase evolution of the two-point spatial correlation functions, R_{uu} and R_{vv}, along with linear stochastic estimates of the phase-dependent velocity field in the presence of a swirling strength event in the log layer are presented. The results reveal a flowfield that is dominated by very large-scale but decaying turbulence events in the early stages of the cycle acceleration phase, which is followed by a brief period of relaminarized flow in the presence of a strong acceleration. Turbulence

reemerges in the later portions of the cycle acceleration phase. Hairpin-packet signatures that are very similar to those described by Christensen and Adrian [21] appear in the stochastically estimated velocity fields ranging from the later ~1/3 of the cycle acceleration stage through the first ~2/3 of the deceleration phase. An approximate mean vortex spacing of $x/H \sim 0.4$ is suggested by the stochastically estimated fields, which is consistent with earlier observations made in steady channel flows over a wide range of Reynolds numbers.

Acknowledgments

Sandia is a multiprogram laboratory operated by Sandia Corporation, a Lockheed-Martin Company, for the United States Department of Energy's National Nuclear Security Administration under Contract DE-AC04-94AL85000. This work was funded by the Strategic Environmental Research and Development Program (SERDP) and the Environmental Security Technology Certification Program (ESTCP). SERDP is the Department of Defense's (DoD) environmental science and technology program, planned and executed in full partnership with the Department of Energy and the Environmental Protection Agency, with participation by numerous other federal and non-federal organizations. ESTCP is a Department of Defense (DoD) program that promotes innovative, cost-effective environmental technologies through demonstration and validation at DoD sites.

References

1 Jepsen, R., Roberts, J., and Gailani, J., "Erosion Measurements in Linear, Oscillatory, and Combined Oscillatory and Linear Flow Regimes," *Journal of Coastal Research*, Vol. 20, 2004, pp. 1096-1101.

2 Kearney, S. P., Jacobi, A. M., and Lucht, R. P., "Time-Resolved Thermal Boundary Layer Structure in a Pulsatile Reversing Channel Flow," *Journal of Heat Transfer*, Vol. 123, 2001, pp. 655-664.

3 Uchida, S., "The Pulsating Viscous Flow Superposed on the Steady Laminar Motion of Incompressible Fluid in a Circular Pipe," *Zeitschrift für Angewandte Mathematik und Physik (ZAMP)*, Vol. 7, 1956, pp. 403-422.

4 Currie, I. G., *Fundamental Mechanics of Fluids*, 2nd ed. New York: McGraw-Hill, 1993.

5 Muntges, D. E. and Majdalani, J., "Pulsatory Channel Flow for an Arbitrary Volumetric Flowrate, AIAA 2002-2856," 32nd AIAA Fluid Dynamics Conference, St. Louis. MO, 2002.

6 S.Ray, Ünsal, B., Durst, F., Ertunc, Ö., and Bayoumi, O. A., "Mass Flow Rate Controlled Fully Developed Laminar Pulsating Pipe Flows," *Journal of Fluids Engineering*, Vol. 127, 2005, pp. 405-418.

7 Hino, M., Kashiwayanagi, M., Nakayama, A., and Hara, T., "Experiments on the Turbulence Statistics and the Structure of a Reciprocating Oscillatory Flow," *Journal of Fluid Mechanics*, Vol. 131, 1983, pp. 363-400.

8 Akhavan, R., Kamm, R. D., and Shapiro, A. H., "An Investigation of Transition to Turbulence in Bounded Oscillatory Stokes Flows Part 1. Experiments," *Journal of Fluid Mechanics*, Vol. 225, 1991, pp. 395-422.

9 Jensen, B. L., Sumer, B. M., and Fredsoe, J., "Turbulent Oscillatory Boundary Layers at High Reynolds Numbers," *Journal of Fluid Mechanics*, Vol. 206, 1989, pp. 265-297.

10 Kearney, S. P., O'Hern, T. J., Dimiduk, T. G., Grasser, T. W., Barney, J., and Roberts, J. D., "Particle-Image Velocimetry Investigation of an Oscillating Turbulent Channel Flow, AIAA 2008-693," 46th AIAA Aerospace Sciences Meeting and Exhibit, Reno, NV, 2008.

11 Scotti, A. and Piomelli, U., "Numerical Simulation of Pulsating Turbulent Channel Flow," *Physics of Fluids*, Vol. 13, 2001, pp. 1367-1384.

12 Costamagna, P., Vittori, G., and Blondeaux, P., "Coherent Structures in Oscillatory Boundary Layers," *Journal of Fluid Mechanics*, Vol. 474, 2003, pp. 1-33.

13 Salon, S., Armenio, V., and Crise, A., "A Numerical Investigation of the Stokes Boundary Layer in the Turbulent Regime," *Journal of Fluid Mechanics*, Vol. 570, 2007, pp. 253-296.

14 Cantwell, B. J., "Organized motion in Turbulent Flow," *Annual Review of Fluid Mechanics*, Vol. 13, 1981, pp. 457-515.

15 Adrian, R. J., "Hairpin Vortex Organization in Wall Turbulence," *Physics of Fluids*, Vol. 19, 2007, pp. 041301.

16 Fishler, L. S. and Brodkey, R. S., "Transition, Turbulence and Oscillating Flow in a Pipe," *Experiments in Fluids*, Vol. 11, 1991, pp. 388-398.

17 Sarpkaya, T., "Coherent Structures in Oscillatory Boundary Layers," *Journal of Fluid Mechanics*, Vol. 253, 1993, pp. 105-140.

18 White, F. M., *Viscous Fluid Flow*, 2nd ed. New York: McGraw-Hill, 1991.

19 Adrian, R. J., Christensen, K. T., and Liu, Z. C., "Analysis and Interpretation of Instantaneous Turbulent Velocity Fields," *Experiments in Fluids*, Vol. 29, 2000, pp. 275-290.
20 Adrian, R. J., Meinhart, C. D., and Tomkins, C. D., "Vortex Organization in the Outer Region of the Turbulent Boundary Layer," *Journal of Fluid Mechanics*, Vol. 422, 2000, pp. 1-54.
21 Christensen, K. T., Wu, Y., Adrian, R. J., and Lai, W., "Statistical Imprints of Structure in Wall Turbulence, AIAA 2004-1116," 42nd Aerospace Sciences Meeting and Exhibit, Reno, NV, 2004.
22 Christensen, K. T. and Adrian, R. J., "Statistical Evidence of Hairpin Vortex Packets in Wall Turbulence," *Journal of Fluid Mechanics*, Vol. 431, 2001, pp. 433-443.